Kinetics of the Reaction $C_2H_5 + HO_2$ by Time-Resolved Mass Spectrometry†

Wiebke Ludwig, Björn Brandt, Gernot Friedrichs,*,‡ and Friedrich Temps*,§

Institut für Physikalische Chemie, Olshausenstr. 40, Christian-Albrechts-Universität zu Kiel, D-24098 Kiel, Germany

Received: October 9, 2005; In Final Form: December 13, 2005

The overall rate constant for the radical−radical reaction $C_2H_5 + HO_2 \rightarrow$ products has been determined at room temperature by means of time-resolved mass spectrometry using a laser photolysis/flow reactor combination. Excimer laser photolysis of gas mixtures containing ethane, hydrogen peroxide, and oxalyl chloride was employed to generate controlled concentrations of C_2H_5 and HO_2 radicals by the fast H abstraction reactions of the primary radicals Cl and OH with C_2H_6 and H_2O_2, respectively. By careful adjustments of the radical precursor concentrations, the title reaction could be measured under almost pseudo-first-order conditions with the concentration of HO_2 in large excess over that of C_2H_5. From detailed numerical simulations of the measured concentration−time profiles of C_2H_5 and HO_2, the overall rate constant for the reaction was found to be $k_1(293\ \mathrm{K}) = (3.1 \pm 1.0) \times 10^{13}\ \mathrm{cm^3\ mol^{-1}\ s^{-1}}$. C_2H_5O could be confirmed as a direct reaction product.

1. Introduction

Reactions of peroxy radicals ($RO_2^\bullet$) are known to play decisive roles in low-temperature combustion processes, flame propagation, and fuel self-ignition, which causes engine knocking. In a simplified generic form, the reaction scheme for low-temperature hydrocarbon oxidation is often written as[1,2]

$$R^\bullet + O_2 \rightleftharpoons RO_2^\bullet$$

$$RO_2^\bullet + RH \rightarrow ROOH + R^\bullet$$

$$ROOH \rightarrow RO^\bullet + {}^\bullet OH$$

$$RO_2^\bullet \rightarrow Q^\bullet OOH$$

$$Q^\bullet OOH \rightarrow \text{cyclic-RO} + {}^\bullet OH$$

$$Q^\bullet OOH + O_2 \rightarrow\rightarrow \text{chain branching}$$

The initial step is the formation of $RO_2^\bullet$ from an alkyl radical $R^\bullet$ and molecular oxygen. The strong temperature dependence of the $R^\bullet + O_2 \rightleftharpoons RO_2^\bullet$ equilibrium is believed to be the main cause of the observed negative temperature coefficient (NTC) of alkane ignition at temperatures above 600 K.[2] In the following reaction, the $RO_2^\bullet$ radical can attack the fuel RH, producing the hydroperoxide ROOH. Subsequent dissociation of the ROOH to $RO^\bullet + {}^\bullet OH$ is a primary chain branching step that is responsible for ignition. Alternatively, the peroxy radical $RO_2^\bullet$ undergoes an internal H atom shift to form the hydroperoxyalkyl radical $Q^\bullet OOH$, which is believed to be the precursor for a number of partially oxidized compounds, including cyclic ethers (cyclic-RO) like ethylene oxide. Eventually, consecutive reaction steps of the $Q^\bullet OOH$ radical with O_2 are thought to lead to additional chain branching.

Considering ethane (i.e., $R = C_2H_5$) as model fuel, however, recent studies have indicated that this mechanism may be incomplete.[3−5] As a result of those studies, the radical−radical reaction

$$C_2H_5 + HO_2 \rightarrow C_2H_5O + OH \qquad (1a)$$

was proposed as a further, new chain branching source. Schaefer et al.[3,4] revisited the ethyl + O_2 system and identified a new concerted elimination pathway, by which ethylperoxy can produce HO_2,

$$C_2H_5O_2 \rightarrow C_2H_4 + HO_2 \qquad (2a)$$

This reaction may also be important for larger alkyl peroxy radicals. However, for small hydrocarbons the barrier for HO_2 elimination (2a) was found to be significantly lower than that for the isomerization reaction

$$C_2H_5O_2 \rightarrow CH_2CH_2OOH \qquad (2b)$$

so that (2a) successfully competes with the intramolecular H transfer (2b). Carstensen et al.[5] pointed out several implications of this finding for the low-temperature oxidation of alkanes. Due to the low reactivity toward fuel molecules, the concentration of HO_2 may build up to a point where fast radical−radical reactions such as reaction 1a start to take off. Considering the above generic ignition mechanism, reactions with alkyl radicals,

$$R^\bullet + HO_2 \rightarrow RO^\bullet + {}^\bullet OH$$

become of considerable interest because they lead to a feedback on the $R^\bullet + O_2 \rightleftharpoons RO_2^\bullet$ equilibrium and constitute a potential further chain branching source. In consecutive steps, the alkoxy radicals $RO^\bullet$ will either dissociate to a smaller alkyl radical and a corresponding carbonyl compound or react with excess O_2 to regenerate HO_2 and a reactive aldehyde or ketone.

Further evidence for a prominent role of alkyl + HO_2 reactions comes from a very recent sensitivity study of two-stage hydrocarbon ignition. On the basis of the comprehensive mechanism for low-temperature *n*-heptane oxidation given by Curran et al.,[6] Kazakov et al.[7] performed a sensitivity, mass

† Part of the special issue "Jürgen Troe Festschrift".

* To whom correspondence should be addressed.
‡ Email: gfriedr@phc.uni-kiel.de
§ E-mail: temps@phc.uni-kiel.de

10.1021/jp0557464 CCC: $33.50
Published on Web 01/19/2006

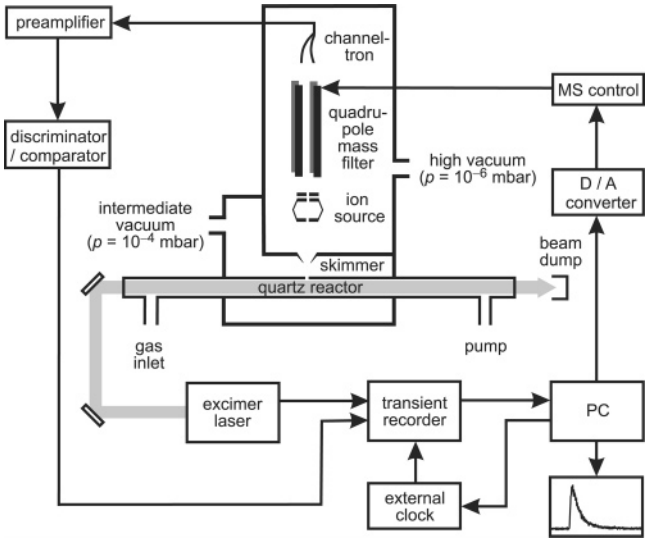

Figure 1. Schematic diagram of the experimental setup.

flux and eigenvalue analysis of *n*-heptane/air ignition. In the NTC region, next to the formation/dissociation of H_2O_2 and the isomerization of the heptyl peroxy radical, the $C_2H_5 + HO_2$ reaction 1a was found to be among the most sensitive reactions for the observed total ignition delay.

In the present publication, we report on a first direct measurement of the overall rate constant for the reaction of C_2H_5 with HO_2,

$$C_2H_5 + HO_2 \rightarrow \text{products} \qquad (1)$$

Assuming a recombination-elimination mechanism, reaction 1 likely yields $C_2H_5O + OH$ (1a) as major products and thus induces chain branching.

We investigated reaction 1 at room temperature by means of laser photolysis and time-resolved mass spectrometry (LP/TRMS). Controlled concentrations of HO_2 and C_2H_5 were generated by ArF excimer laser photolysis of mixtures of ethane, hydrogen peroxide, and oxalyl chloride diluted in He through the reactions of the photolysis products OH and Cl with H_2O_2 and C_2H_6. The concentrations of HO_2 were kept in large excess compared to those of C_2H_5. The overall reaction rate constant was determined from the measured C_2H_5 and HO_2 concentration−time profiles by detailed numerical simulations. The reaction product C_2H_5O was detected at mass signals $m/z = 45$ ($C_2H_5O^+$) and $m/z = 43$ (fragment $C_2H_3O^+$).

2. Experimental Section

A schematic diagram of the experimental setup is shown in Figure 1. The measurements were carried out in a 65 cm long, 1.7 cm i.d. quartz reactor connected to a molecular beam sampling quadrupole mass spectrometer (Extrel C50, Bruker MM1). Spatially homogeneous concentrations of radicals in the reactor were produced by excimer laser (Lambda Physik Compex 102, $\lambda = 193$ nm) photolysis of suitable precursor molecules. The laser beam was directed along the reactor axis using dielectric mirrors and was spatially filtered by 1.5 cm i.d. apertures to ensure a homogeneous radial intensity profile. The fused quartz windows at both ends of the reactor were purged with He to prevent carbon deposition. The laser pulse energies measured with a calibrated pyroelectric detector (Coherent LM-P10i) before the entrance and behind the exit window were between 25 and 45 mJ (average of incident and transmitted values). The excimer laser was operated at a repetition rate of 5 Hz and the measurements were carried out under slow flow conditions to replace the gas volume in the reactor between laser shots. Helium was used as the inert carrier gas. The gas pressure in the reactor was measured with a capacitance pressure transducer (MKS Baratron). All measurements were carried out at a total pressure of $p = 1.2$ mbar and at room temperature (293 K). The reactor was cleaned using a 5% aqueous solution of HF and thoroughly rinsed with distilled water prior to installation.

Samples of the gas mixture in the reactor continuously expanded through a 0.7 mm conical pinhole in the reactor wall and a 0.5 mm skimmer into the differentially pumped high vacuum chamber ($p = 10^{-6}$ mbar) of the mass spectrometer. Molecular ions were generated by low energy electron impact ionization ($E(C_2H_5) = 11.5$ eV, $E(HO_2) = 15.5$ or 21.5 eV, $E(HCl) = 14.2$ eV, $E((COCl)_2) = 17.5$ eV). The ions were extracted at right angles, mass filtered using a quadrupole analyzer, and monitored using a channeltron detector connected via a preamplifier (Stanford Research SR445) and a discriminator/comparator circuit to a transient recorder PC card (Spectrum PAD280A) for single ion counting and averaging. Signals from 5000 to 10 000 laser shots were accumulated to record the kinetic concentration−time profiles at a selected *m*/*z* setting. The applied electron impact energies were a compromise between a sufficient signal-to-noise ratio and the desired background suppression. For further data analysis, the signals were baseline corrected by subtracting the measured pretrigger background fragmentation signal levels. The mass spectrometer settings and data aquisition were controlled by a microcomputer running LabView software.

The gases He (99.996%), C_2H_6 (99.5%), and O_2 (99.995%, Messer-Griesheim) were used as supplied. $(COCl)_2$ (98%, Aldrich) and, for calibration purposes, CH_3OH (99.9%, Merck) and $CFCl_3$ (99%, Aldrich) were degassed prior to use by repeated freeze−pump−thaw cycles. HCl was obtained from NaCl and H_2SO_4 (95%) and was purified by distillation. The gas flows were regulated by means of calibrated mass flow controllers (Aera). Gas mixtures were prepared by partial pressures in a glass mixing system and were allowed to mix thoroughly, typically overnight, before use. H_2O_2 was generated by thermal decomposition of a urea hydrogen peroxide adduct (Lancester, 97%). A mixture of sand (to reduce crust formation) and the substance was kept in a thermostated flask to allow us to control the H_2O_2 vapor pressure by variation of the temperature. A constant gas flow of He was flushed through the flask, resulting in a steady-state concentration of H_2O_2 in the carrier gas which was directly fed into the reactor for the kinetic measurements. The concentration in the carrier gas flow was determined by collecting the H_2O_2 in a cryo trap for a specific time followed by titration with $KMnO_4$. The setup provided stable H_2O_2 concentrations for several hours. At elevated decomposition temperatures, small amounts of H_2O and O_2 were detected indicating a beginning decomposition of H_2O_2. Therefore, the working temperatures were kept as low as possible (30−55 °C) to suppress H_2O and O_2.

A modified version of the Chemkin-II package,[8] which was also capable of fitting rate constants by a nonlinear Levenberg−Marquardt fitting routine, was used for numerical simulations. For the comparison of numerical simulation and experiment, the calculated concentration−time profiles were convoluted with the response function of the experimental setup. The response function and corresponding time constant of the setup ($\tau = 0.5$ ms), which is composed of the flight time of the detected ions, the bandwidth of the detection electronics and the transversal diffusional mixing of the gas mixture within the reactor, were

extracted from the rise time of mass signals of stable products obtained by laser photolysis.[9]

3. Results

3.1. Radical Generation. The need for a simultaneous generation of two different radical species constitutes a major problem for measurements of rate constants of radical−radical cross reactions. Moreover, the possibility of competing radical self-reactions or reactions of the radicals with precursor or product molecules requires a subtle control of the experimental conditions. In this work, the radicals C_2H_5 and HO_2 were generated by ArF excimer laser photolysis ($\lambda = 193$ nm) of mixtures containing $(COCl)_2$, H_2O_2, and C_2H_6. Photolysis of $(COCl)_2$ and H_2O_2 yields the primary radicals Cl and OH and, to a lesser extent, also H atoms and HO_2 radicals according to

$$(COCl)_2 + h\nu \rightarrow 2CO + 2Cl \qquad \Phi = 2.0 \qquad (3)$$

$$H_2O_2 + h\nu \rightarrow 2OH \qquad \Phi = 0.85 \qquad (4a)$$

$$\rightarrow H + HO_2 \qquad \Phi = 0.15 \qquad (4b)$$

The quantum yields and the absorption cross sections, $\sigma((COCl)_2) = 3.83 \times 10^{-18}$ cm^2 and $\sigma(H_2O_2) = 6.00 \times 10^{-19}$ cm^2, are well-known.[10,11] The primary radicals are then converted rapidly into the secondary radicals C_2H_5 and HO_2 via the H atom abstraction reactions

$$Cl + C_2H_6 \rightarrow HCl + C_2H_5 \qquad k_5 = 3.6 \times 10^{13}\ \text{cm}^3\ \text{mol}^{-1}\ \text{s}^{-1} \qquad (5)$$

$$Cl + H_2O_2 \rightarrow HCl + HO_2 \qquad k_6 = 2.5 \times 10^{11}\ \text{cm}^3\ \text{mol}^{-1}\ \text{s}^{-1} \qquad (6)$$

$$OH + C_2H_6 \rightarrow H_2O + C_2H_5 \qquad k_7 = 1.5 \times 10^{11}\ \text{cm}^3\ \text{mol}^{-1}\ \text{s}^{-1} \qquad (7)$$

$$OH + H_2O_2 \rightarrow H_2O + HO_2 \qquad k_8 = 1.0 \times 10^{12}\ \text{cm}^3\ \text{mol}^{-1}\ \text{s}^{-1} \qquad (8)$$

At comparable initial concentrations of C_2H_6 and H_2O_2, because the rate constant for the Cl atom reaction (5) with ethane is 144 times larger than the corresponding rate constant with hydrogen peroxide (6), the Cl atoms are almost quantitatively converted into C_2H_5 radicals. Similarly, with $k_8/k_7 = 6.7$, the OH radicals are mainly transformed into HO_2 radicals via reaction 8. Furthermore, under the experimental conditions used in this work, the H atoms generated in the photolysis channel 4b are converted into OH radicals,

$$H + HO_2 \rightarrow 2OH \qquad (9a)$$

$$H + H_2O_2 \rightarrow OH + H_2O \qquad (10a)$$

and thus also yielded HO_2. This kinetic separation of the C_2H_5 and HO_2 formation pathways allowed for a straightforward control of the absolute radical concentrations by simply adjusting the relative initial concentrations of C_2H_6 and $(COCl)_2$ versus that of H_2O_2. Starting from initial concentrations of 2.9×10^{-10} mol cm^{-3} < $[H_2O_2]_0$ < 1.6×10^{-9} mol cm^{-3} and 1.8×10^{-10} mol cm^{-3} < $[C_2H_6]_0$ < 5.3×10^{-10} mol cm^{-3}, HO_2 concentrations of 1.5×10^{-12} to 13×10^{-12} mol cm^{-3} and C_2H_5 concentrations of 1.4×10^{-13} to 21×10^{-13} mol cm^{-3} were readily attained.

3.2. Absolute Radical Concentrations. For a quantitative analysis of the experimental concentration−time profiles, the absolute radical concentrations of C_2H_5 and HO_2 had to be accurately known. In particular, because the concentrations of HO_2 were kept in large excess compared to those of C_2H_5 to enable near pseudo-first-order conditions, the precision of the HO_2 concentration directly limits the accuracy of the rate constant determination. On the basis of four different and complementary methods for the radical concentration determination, absolute radical concentrations could be ensured to be accurate within ±15%.

(i) Photolysis Yields. Assuming that the absorption cross sections of the precursor molecules and the radical quantum yields are accurately known, the primary radical concentrations [Cl] and [OH] could be directly calculated from the measured photolysis laser energy fluence and precursor concentrations. The concentrations of C_2H_5 and HO_2 thus followed according to reactions 5−8.

(ii) Quantitative Detection of Stable Products. A quantitative conversion of atoms or radicals into stable products combined with a direct calibration of the experimental mass signals of the stable products allows for an independent accurate determination of the atom/radical concentrations. In our case, the photolysis of gas mixtures of $(COCl)_2$ and C_2H_6 in He was used to generate Cl atoms that were quantitatively converted to HCl via

$$Cl + C_2H_6 \rightarrow HCl + C_2H_5 \qquad (5)$$

$$Cl + C_2H_5 \rightarrow HCl + C_2H_4 \qquad (11)$$

Figure 2a depicts a time-resolved mass signal at $m/z = 36$ (HCl^+). The observed, baseline corrected HCl signals could be directly related to signals obtained using pure HCl/He calibration mixtures. Ideally, the determined Cl atom concentration is equal to the radical concentration calculated from the photolysis yield.

(iii) $(COCl)_2$ Signal Decrease. The absolute Cl atom concentrations could also be verified on the basis of time-resolved mass signals at $m/z = 126$ ($(COCl)_2^+$). As shown in Figure 2b, following the photolysis laser pulse at $t = 0$ the signal decreases steplike and the relative signal decrease could be taken as a direct measure of the $(COCl)_2$ consumption. No background signal was expected at this mass. However, an additional absolute calibration of the mass signal by using pure $(COCl)_2$/He mixtures was performed to rule out baseline issues. The $(COCl)_2$ mass signal decrease was found to be the most reliable and also most convenient way to determine the photolysis laser energy fluence in the reactor, which could then be used to calculate the absolute photolysis yields of all primary radicals in the kinetic measurements.

(iv) Calibration of HO_2 via the Photolysis of $CH_3OH/O_2/CFCl_3$. The photolysis of gas mixtures containing CH_3OH, O_2, and $CFCl_3$ was applied as an independent way to calibrate the HO_2 mass signals. The initially generated Cl atoms were quantitatively transformed into HO_2 via the reaction sequence

$$CFCl_3 + h\nu \rightarrow CFCl_2 + Cl \qquad (12a)$$

$$\rightarrow CFCl + 2Cl \qquad (12b)$$

$$Cl + CH_3OH \rightarrow HCl + CH_2OH \qquad (13)$$

$$CH_2OH + O_2 \rightarrow HO_2 + CH_2O \qquad (14)$$

In these experiments, $CFCl_3$ was used instead of $(COCl)_2$ as

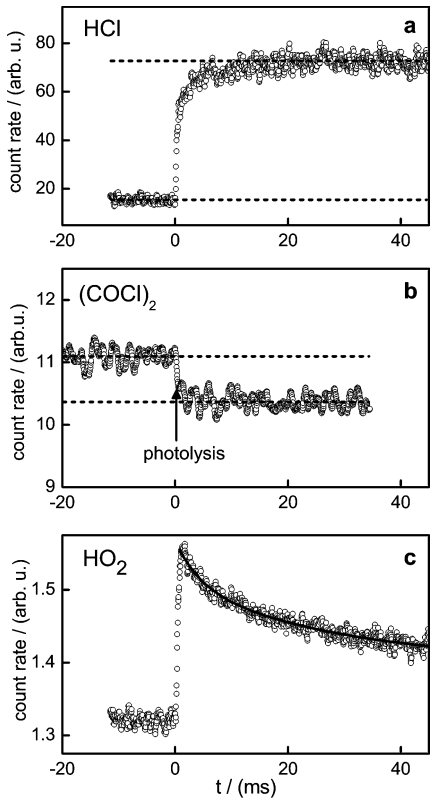

Figure 2. Determination of absolute radical concentrations. (a) Quantitative detection of stable products: Time-resolved mass signals at $m/z = 36$ (HCl^+). (b) Consumption of precursor molecules: Time-resolved mass signals at $m/z = 126$ ($(COCl)_2^+$). (c) Calibration of the HO_2 radical concentration: Time-resolved mass signals at $m/z = 33$ (HO_2^+) for a photolysis experiment with $[CH_3OH]_0 = 2.4 \times 10^{-10}$ mol cm^{-3}, $[O_2]_0 = 1.6 \times 10^{-9}$ mol cm^{-3}, $[Cl]_0 = 3.6 \times 10^{-12}$ mol cm^{-3} together with a kinetic simulation of the HO_2 concentration−time profile in the $CH_3OH/O_2/Cl$ reaction system.

the Cl atom source because $(COCl)_2$ did not provide a good reproducibility in reaction systems containing CH_3OH, presumably because of heterogeneous reactions between $(COCl)_2$ and CH_3OH in the supply lines and on the reactor walls. The absorption cross section of $CFCl_3$, $\sigma(193\text{ nm}) = 1.35 \times 10^{-18}$ cm^{-2} and the overall Cl atom quantum yield of $\phi = 1.23$ are well-known.[11] Figure 2c depicts the time-resolved mass signals at $m/z = 33$ (HO_2^+) for an experiment with $[CH_3OH]_0 = 2.4 \times 10^{-10}$ mol/cm^3, $[O_2]_0 = 1.6 \times 10^{-9}$ mol/cm^3, and $[Cl]_0 = 3.6 \times 10^{-12}$ mol/cm^3 as an example. The extrapolated, baseline corrected HO_2 signal at $t = 0$ corresponds to an HO_2 concentration that is equal to the initial Cl atom photolysis yield. On the basis of the calibration of the HO_2 mass signal, we could thus determine the absolute yield of HO_2 radicals following the photolysis of pure mixtures of H_2O_2. In that case, however, primarily due to the additional HO_2 loss reaction

$$OH + HO_2 \rightarrow H_2O + O_2, \qquad (15)$$

the initially generated OH radicals and H atoms, reactions 4a and 4b, were not quantitatively converted into HO_2 radicals. Therefore, the HO_2 concentration−time profiles had to be numerically simulated by a more complex reaction mechanism, as will be described in more detail below. In any case, comparison of the simulated HO_2 concentrations based on the photolysis yield from the H_2O_2 photolysis (4) with the calibrated absolute HO_2 concentrations from the photolysis of $CH_3OH/O_2/CFCl_3$ showed agreement to within ±10%.

TABLE 1: Room Temperature Reaction Mechanism Used for Numerical Simulations

no.	reaction			k/ cm^3 mol^{-1} s^{-1}	ref
5	$Cl + C_2H_6$	→	$HCl + C_2H_5$	3.6×10^{13}	11
7	$OH + C_2H_6$	→	$H_2O + C_2H_5$	1.5×10^{11}	11
18	$H + C_2H_6$	→	$H_2 + C_2H_5$	2.7×10^{07}	12
8	$OH + H_2O_2$	→	$H_2O + HO_2$	1.0×10^{12}	11
6	$Cl + H_2O_2$	→	$HCl + HO_2$	2.5×10^{11}	11
10a	$H + H_2O_2$	→	$OH + H_2O$	2.5×10^{10}	12
10b		→	$H_2 + HO_2$	3.1×10^{09}	12
19	$C_2H_5 + H_2O_2$	→	$C_2H_6 + HO_2$	1.7×10^{09}	13
1, 1a	$C_2H_5 + HO_2$	→	$C_2H_5O + OH$	3.1×10^{13}	this work
11	$Cl + C_2H_5$	→	$HCl + C_2H_4$	1.5×10^{14}	14
20	$OH + C_2H_5$	→	products	7.1×10^{13}	15
21a	$H + C_2H_5$	→	$H_2 + C_2H_4$	1.8×10^{12}	13
21b		→	$2\ CH_3$	3.6×10^{13}	13
22	$C_2H_5 + C_2H_5$	→	products	1.2×10^{13}	16
23	C_2H_5 + wall	→	products	4−16 s^{-1}	this work
15	$OH + HO_2$	→	$H_2O + O_2$	4.8×10^{13}	11
24a	$Cl + HO_2$	→	$HCl + O_2$	2.1×10^{13}	11
24b		→	$ClO + OH$	5.6×10^{12}	11
9a	$H + HO_2$	→	$2\ OH$	4.3×10^{13}	11
9b		→	$H_2 + O_2$	3.4×10^{12}	11
9c		→	$O + H_2O$	1.5×10^{12}	11
16	$HO_2 + HO_2$	→	$H_2O_2 + O_2$	1.0×10^{12}	11
17	HO_2 + wall	→	products	5−30 s^{-1}	this work
25	Cl + wall	→	products	2 s^{-1}	estimated
26	OH + wall	→	products	25 s^{-1}	estimated
27	OH + HCl	→	$H_2O + Cl$	4.8×10^{11}	11

3.3. Rate Measurements for the Reaction $C_2H_5 + HO_2$. The overall rate constant of the radical−radical cross reaction

$$C_2H_5 + HO_2 \rightarrow \text{products} \qquad (1)$$

was measured at room temperature ($T = 293$ K) and a total pressure of $p = 1.2$ mbar by generating controlled concentration levels of C_2H_5 and HO_2. The experimental conditions were chosen such that the reaction could be studied under conditions with the concentration of HO_2 in large excess over C_2H_5 ($3 < [HO_2]/[C_2H_5] < 20$). In each experimental run, the following five different concentration−time profiles were recorded: (i) A $(COCl)_2$ profile was measured to determine the $[Cl]_0$ concentration, the photolysis laser energy fluence, and with it the absolute radical yield (see section 3.2). (ii, iii) HO_2 and C_2H_5 reference profiles were obtained by the photolysis of mixtures of H_2O_2 in He or C_2H_6 and $(COCl)_2$ in He, respectively. These reference profiles, which are free from contributions of the cross reaction 1, were used to determine the absolute HO_2 radical yield and the wall loss rate constants of HO_2 and C_2H_5. (iv, v) Finally, HO_2 and C_2H_5 profiles were measured following the photolysis of mixtures of H_2O_2, C_2H_6, and $(COCl)_2$. Observed differences between these and the corresponding reference concentration−time profiles should be essentially attributable to the influence of reaction 1. During the measurement campaign (several weeks) the determined effective wall loss rate constants, which are fairly scattered (see Table 1), showed a slight systematic increase for HO_2 and a slight systematic decrease for C_2H_5. However, for each experimental data point all required measurements (HO_2, C_2H_5, and $(COCl)_2$ profiles) were carried out during 1 day such that appropriate HO_2 and C_2H_5 reference profiles were always available.

Figure 3 illustrates typical HO_2 and C_2H_5 concentration−time profiles for an experiment with $[H_2O_2]_0 = 1.4 \times 10^{-9}$, $[C_2H_6] = 2.7 \times 10^{-10}$, $[Cl]_0 = 5.0 \times 10^{-13}$, $[OH]_0 = 2.0 \times 10^{-11}$, and $[H]_0 = [HO_2]_0 = 1.8 \times 10^{-12}$ (units are mol cm^{-3}). Panel a corresponds to the *unperturbed* HO_2 and C_2H_5 reference profiles, panel b depicts the corresponding *perturbed* profiles

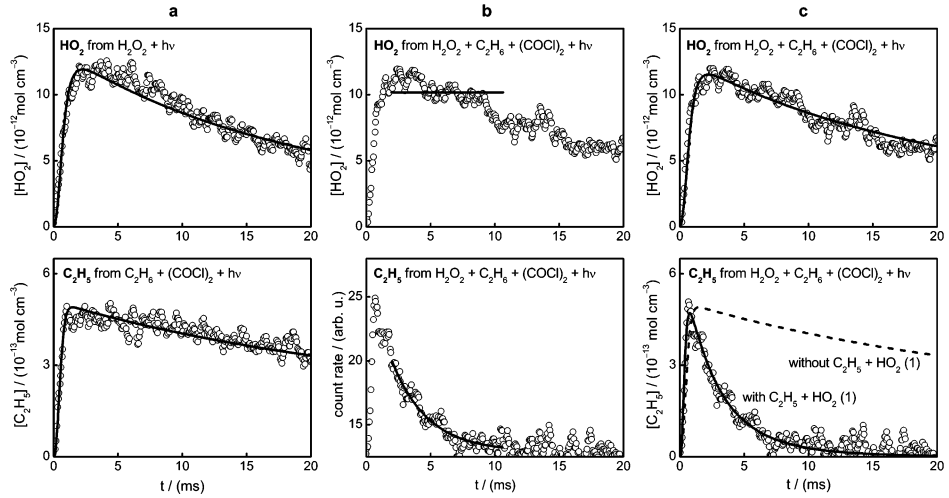

Figure 3. Experimental concentration−time profiles of HO_2 and C_2H_5 obtained from the photolysis of different reaction mixtures (circles). The solid curves correspond to numerical simulations. (a) Reference profiles of HO_2 from H_2O_2/He mixture and of C_2H_5 from C_2H_6/$(COCl)_2$/He mixture. (b) Experimental concentration−time profiles of HO_2 and C_2H_5 from H_2O_2/C_2H_6/$(COCl)_2$/He mixtures and approximate pseudo-first-order evaluation (see text). (c) Experimental signals of HO_2 and C_2H_5 from H_2O_2/C_2H_6/$(COCl)_2$/He mixtures (same as in (b)) together with full numerical simulations based on the reaction mechanism given in Table 1. The dashed curve corresponds to a simulation that completely neglects reaction 1. Experimental conditions are given in Table 2 (experiment no. 9).

with the cross reaction 1 switched on, and panel c shows the results of corresponding numerical simulations. Whereas the initially generated Cl atoms were almost quantitatively converted to C_2H_5 within 1−2 ms, the HO_2 yield had to be numerically simulated by a reaction mechanism (see Table 1) that also takes into account additional HO_2 removal reactions

$$OH + HO_2 \rightarrow H_2O + O_2 \quad (15)$$

$$HO_2 + HO_2 \rightarrow H_2O_2 + O_2 \quad (16)$$

$$HO_2 \rightarrow \text{wall} \quad (17)$$

$$H + HO_2 \rightarrow 2OH \quad (9a)$$

which influence the absolute HO_2 yields. For the example given in Figure 3, the maximum of the HO_2 concentration−time profile corresponds to approximately 50% of the maximum yield that would have been obtained without any interfering HO_2 loss reactions. As becomes clear from a comparison of the signals in panels a and b, however, the addition of C_2H_6, $(COCl)_2$ and C_2H_5 radicals essentially did not change the observed HO_2 concentration−time profile. The small difference of the HO_2 profile confirms the near pseudo-first-order conditions ($[HO_2] > [C_2H_5]$), although the slow decay of the HO_2 concentration with time was unavoidable. On the other hand, in contrast to the excess component HO_2, the C_2H_5 decay became much faster in the presence of HO_2 (see panels b and c). This obvious change in the observed C_2H_5 profiles demonstrates the importance of reaction 1.

Estimation of k_1 from a Pseudo-First-Order Evaluation. Both the minor alteration in the HO_2 signal and the significant change in the overall C_2H_5 decay rate suggest that an approximate pseudo-first-order evaluation of the data is possible to obtain a first estimate for the value of k_1. Figure 4 summarizes the results of such a preliminary evaluation of the data in a plot of the obtained pseudo-first-order rate constants k_1' versus the average HO_2 concentration. The experimental conditions and results are given in Table 2. As it is exemplified in panel b of Figure 3, single-exponential fits to the experimental C_2H_5 profiles were restricted to reaction times $t > 2$ ms (HO_2 formation complete), and mean HO_2 concentrations were determined by averaging

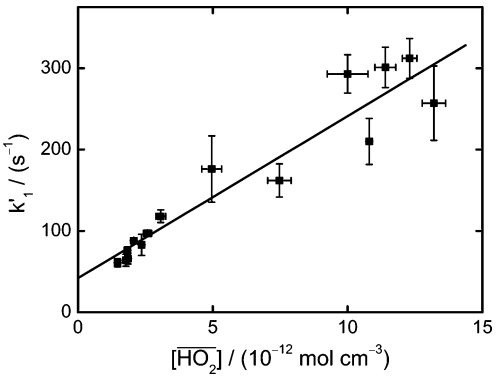

Figure 4. Plot of the pseudo-first-order rate constant $k_1' = k_1[\overline{HO_2}] + k_d$ versus the average $[\overline{HO_2}]$ concentration. The slope of the straight line corresponds to a value of $k_1 = 2.0 \times 10^{13}$ cm^3 mol^{-1} s^{-1}.

the HO_2 profiles over the fitting range. The slope of the straight line through the data in Figure 4 corresponds to a value of the bimolecular rate constant

$$k_1 = (2.0 \pm 0.7) \times 10^{13} \text{ cm}^3 \text{ mol}^{-1} \text{ s}^{-1}$$

The error limit is composed of the 2σ error of the linear regression (±18%) and the error of the absolute HO_2 concentration (±15%). The obtained intercept of $k_d = 42 \pm 26$ s^{-1} confirms an overall small influence of the background reactions, which contribute to the C_2H_5 decay.

Determination of k_1 by Numerical Simulations. Owing to secondary reactions that may have a pronounced influence on the obtained first-order rate constants, the above pseudo-first-order treatment of the data can only be taken as an approximate evaluation. Moreover, the coarse assumption of a time-independent averaged HO_2 concentration does not take the HO_2 chemistry into adequate account. A complete simulation of the observed C_2H_5 and HO_2 concentration−time profiles provided for a more reliable rate constant determination. The applied reaction mechanism was assembled from literature data and is given in Table 1. It includes the most important reactions of Cl, OH, H, C_2H_5, HO_2, and of the precursor species C_2H_6 and H_2O_2. All reactions with known reaction products were verified to proceed predominantly in the specified directions. Provision

TABLE 2: Experimental Conditions and Results

no.	$[C_2H_6]_0/10^{-10}$	$[H_2O_2]_0/10^{-10}$	$[Cl]_0/10^{-13}$	$[OH]_0/10^{-12}$	$[HO_2]_0/10^{-13}$	$[H]_0/10^{-13}$	$\overline{[HO_2]}/10^{-12}$	$\overline{[HO_2]}/[Cl]_0$	k'_1/s^{-1}	$k_1/10^{13}$
1	5.20	4.00	20.5	6.4	5.7	5.7		10		2.81
2	5.29	4.42	10.8	6.1	5.4	5.4	3.1	3	118	3.53
3	3.47	10.9	13.2	19.1	16.8	16.8	13.2	10	257	2.66
4	3.51	6.88	7.6	10.2	9.0	9.0	7.5	10	162	3.43
5	2.69	6.90	5.2	10.1	8.9	8.9	5.0	10	176	3.37
6	2.60	15.5	13.9	21.5	19.0	19.0	11.4	8	301	2.13
7	2.63	15.6	7.1	21.9	19.4	19.4	12.3	17	312	2.63
8	2.63	12.7	15.3	25.8	22.8	22.8	10.8	7	210	1.60
9	2.65	14.2	5.0	20.1	17.7	17.7	10.0	20	293	3.04
10	2.59	3.05	1.4	3.5	3.1	3.1	1.9	14	66	4.23
11	2.52	2.97	2.5	3.2	2.9	2.9	1.5	6	61	4.09
12	1.77	3.61	5.3	6.7	5.9	5.9	2.6	5	97	2.45
13	1.78	3.70	3.2	6.8	6.0	6.0	1.8	6	76	2.68
14	1.84	2.87	3.1	4.3	3.8	3.8	1.8	6	64	3.96
15	1.87	3.70	2.6	5.2	4.6	4.6	2.4	9	83	3.06
16	1.86	3.67	3.3	5.1	4.5	4.5	2.1	6	88	3.51

[a] $T = 293$ K, $p = 1.2$ mbar. k'_1 from pseudo-first-order evaluation (in s^{-1}), k_1 from numerical evaluation (in $cm^3\ mol^{-1}\ s^{-1}$). All concentrations are given in units of mol cm^{-3}.

for the corresponding reverse rate constants, which were calculated from thermodynamic data, did not change the results. The experimental data were analyzed as follows. First, the measured C_2H_5 and HO_2 reference profiles were matched by attributing remaining discrepancies between the simulation and the experimentally observed radical decay to the wall loss reactions (solid curves in panel a of Figure 3). Moreover, the mass spectrometric calibration factors that were used to convert the experimental count-rate vs time signals into radical concentration−time profiles were reassessed from these profiles. The experimental C_2H_5 profiles were then fitted using k_1 as an adjustable parameter (solid curves in panel c of Figure 3). Because the absolute signal heights obtained in repeated experiments were found to fluctuate by ±10%, allowance was made for slight adjustments of the calibration factor in a final fit. Note, however, that small inaccuracies of the absolute C_2H_5 concentrations, which may have been introduced in this way, did not critically enter into the determined rate constant due to the near pseudo-first-order conditions. Furthermore, for each individual experimental trace, the fit procedure was checked to be reliable by choosing six different reasonable fit ranges over which the C_2H_5 decay was observed. The obtained values for the rate constant k_1 agreed to within ±5% and the average of the six determinations was taken as the final k_1 value. Finally, a simulation of the corresponding HO_2 profile was used to verify the consistency of the determined rate data. In most cases, the rate of reaction 1 did not have a pronounced influence on the HO_2 concentrations. Experimental conditions and results are summarized in Table 2. From the average of a total of 16 experiments, the rate constant for reaction 1 was determined to be

$$k_1(293\ \mathrm{K}) = (3.1 \pm 1.0) \times 10^{13}\ \mathrm{cm^3\ mol^{-1}\ s^{-1}}$$

The stated error takes into account the statistical error of the mean (2σ, ±12%), uncertainties due to the absolute HO_2 concentration (±15%), and the estimated combined error due to the applied mechanism and absolute C_2H_5 concentration (±5%). Within the scatter of the data, no systematic variations of the determined rate constants with different initial precursor concentration, radical concentration, or HO_2 excess ratio were discernible.

4. Discussion

The rate constant for reaction 1, $C_2H_5 + HO_2$, was extracted from C_2H_5 concentration−time profiles with the concentration of HO_2 in large excess over that of C_2H_5. In panel c of Figure 3, the comparison of a full simulation (solid curve) with a simulation that completely neglects reaction 1 (dashed curve), reveals the predominant role of this reaction for the experimentally observed C_2H_5 decay. The rate constants obtained using both an approximate pseudo-first-order treatment and a numerical evaluation of the data agree within their specified error limits. However, with $k_1 = (3.1 \pm 1.0) \times 10^{13}\ cm^3\ mol^{-1}\ s^{-1}$, the value from the numerical simulations came out about 50% higher. Therefore, sensitivity and contribution analyses were performed to assess the influence of secondary chemistry.

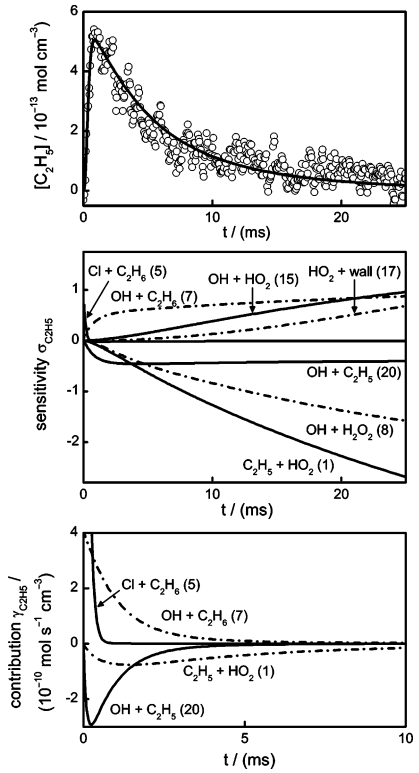

Figure 5. C_2H_5 concentration−time profile (top), corresponding sensitivity analysis (middle), and contribution plot (bottom) for experiment no. 5. Experimental conditions are given in Table 2.

4.1. Sensitivity and Contribution Analyses. Figure 5 displays an experimental C_2H_5 concentration−time profile together with the corresponding contribution plot and sensitivity analysis. With regard to the C_2H_5 and HO_2 concentrations, the

example shown (experiment no. 5 in Table 2) falls into the midrange of experimental conditions applied. The sensitivity analysis of the reaction system was performed by calculating the normalized local sensitivity coefficients $\sigma(i,t) = d(\ln [C_2H_5])/d(\ln k_i)$ of the ith reaction of C_2H_5 at the reaction time t. A contribution plot for C_2H_5 was constructed by calculating the contribution $\gamma_{C_2H_5}(i,t) = k_i[C_2H_5]\Pi_j c(j,t)$ of reaction i at time t, where $c(j,t)$ are the concentrations of the species appearing in the rate law of reaction i next to C_2H_5 itself. For the reaction $C_2H_5 + HO_2$, for example, the contribution is given by $\gamma_{C_2H_5} = k_1[C_2H_5][HO_2]$. High absolute values of the contribution and/or sensitivity coefficient imply that the reaction is important for the numerical modeling of the experimental concentration−time profile.

It becomes apparent from Figure 5 that the rate of reaction 1 dominates the fate of the C_2H_5 radicals at reaction times $t >$ 2−4 ms so that the determination of k_1 is possible. However, next to reaction 1, there are several other reactions influencing the C_2H_5 concentration−time profile. It is obvious that the reactions $Cl + C_2H_6$ (5) and $OH + H_2O_2$ (8) as the main sources for C_2H_5 and HO_2, respectively, exhibit high sensitivities. As is expected for a quantitative conversion of Cl atoms into C_2H_5 radicals, next to reaction 5 no other Cl atom reactions play a significant role. The situation is slightly different with the OH radical. Due to the comparably slow reaction 8 and the permanent regeneration of OH radicals through reaction 1a, several other OH radical reactions cannot be neglected. In particular, the reactions

$$OH + C_2H_6 \rightarrow H_2O + C_2H_5 \quad (7)$$

$$OH + C_2H_5 \rightarrow \text{products} \quad (20)$$

have a pronounced influence on the absolute C_2H_5 and HO_2 yields at shorter reaction times, whereas the reaction

$$OH + HO_2 \rightarrow H_2O + O_2 \quad (15)$$

gains importance at a later stage of the overall reaction. Despite this somewhat complex chemistry, the simple pseudo-first-order treatment of the data yielded about the right rate constant value. This is due to the fact that (i) the influence of the secondary reactions on the absolute HO_2 yield has been approximately taken into account by the independent determination of the absolute HO_2 yield and (ii) the influences of C_2H_5 consuming and generating reactions (e.g., reaction 20 vs reaction 7) partly compensate each other. The same arguments hold for the accuracy of the numerical evaluation. Because both the reaction mechanism was shown to accurately predict the absolute concentration of the HO_2 radicals and the rate constants of the most important secondary reactions are well-known from the literature, the rate constant for reaction 1 could be reliably determined from the experiments.

The only problematic rate constant, which is based on only a single measurement, is that of the radical cross reaction OH + C_2H_5 (20). Fagerström et al. investigated this reaction by means of pulse radiolysis of mixtures of $C_2H_6/H_2O/SF_6$ and monitoring of C_2H_5 and CH_3 radicals by UV absorption at 205 and 216 nm.[15] At pressures of 250 mbar $< p <$ 1000 mbar, a pressure independent total rate constant of $k_{20} = 7.1 \times 10^{13}$ cm^3 mol^{-1} s^{-1} was reported. Assuming a recombination−elimination mechanism, at the low pressures used in this study, reaction 20 likely yields $C_2H_4 + H_2O$ as major products. To assess the influence of reaction 20 on the determined rate constant k_1, numerical simulations were carried out with $k_{20} \pm$ 50%. These variations could be compensated by a much smaller variation of $k_1 \mp 10\%$ within error limits. Altogether, in the light of the foregoing discussion, the detailed numerical simulation adequately takes into account the influence of secondary chemistry and is therefore preferred to the approximate pseudo-first-order result.

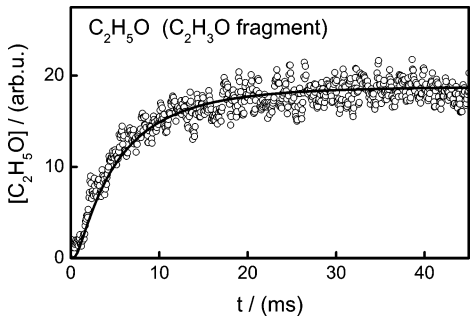

Figure 6. Product profile at $m/z = 43$ corresponding to the C_2H_3O fragment of C_2H_5O. The solid curve represents a scaled numerical simulation of C_2H_5O based on the mechanism given in Table 1.

4.2. Reaction Products. Possible product channels of reaction 7 are (thermodynamic data are taken from ref 17)

$$C_2H_5 + HO_2 \rightarrow C_2H_5O + OH \qquad \Delta_r H^\circ_{298} = -108 \text{ kJ mol}^{-1} \quad (1a)$$

$$\rightarrow CH_3 + CH_2O + OH \qquad \Delta_r H^\circ_{298} = -56 \text{ kJ mol}^{-1} \quad (1b)$$

$$\rightarrow H + CH_3CHO + OH \qquad \Delta_r H^\circ_{298} = -42 \text{ kJ mol}^{-1} \quad (1c)$$

$$\rightarrow C_2H_5OH + O \qquad \Delta_r H^\circ_{298} = -117 \text{ kJ mol}^{-1} \quad (1d)$$

$$\rightarrow H_2O_2 + C_2H_4 \qquad \Delta_r H^\circ_{298} = -215 \text{ kJ mol}^{-1} \quad (1e)$$

$$\rightarrow O_2 + C_2H_6 \qquad \Delta_r H^\circ_{298} = -215 \text{ kJ mol}^{-1} \quad (1f)$$

Assuming a recombination−elimination mechanism, as outlined by Troe,[18] reaction 1 likely yields $C_2H_5O + OH$ (1a) as major products. Allowing for a possible decomposition of the C_2H_5O radicals, $CH_3 + CH_2O + OH$ (1b) or, less favorably,[19] $H + CH_3CHO + OH$ (1c) may be minor products. Although thermodynamically feasible, the formation of $C_2H_5OH + O$ is very unlikely due to the required major rearrangement steps of the initially formed $C_2H_5OOH^*$ association complex. In addition, there are two H atom transfer pathways 1e and 1f taken into account for completeness. Because the *loose* (i.e., simple bond fission) channel 1a is energetically lower than the energy of the $C_2H_5OOH^*$ complex and does not exhibit an additional energy barrier, one can conclude that the overall reaction will be essentially association-controlled and that no pressure dependence will be discernible at the mbar pressures applied. Of course, toward markedly higher pressures, collisional deactivation of the complex will become important eventually. Pertaining to hydrocarbon self-ignition, channels 1a−1c induce chain branching, whereas channels 1e and 1f result in a quenching of radicals and inhibition.

Product measurements carried out in this work support the assumption that channel 1a is a major product channel. Figure 6 shows a strong mass signal detected on the mass of C_2H_3O ($m/z = 43$). C_2H_3O constitutes a main mass fragment of C_2H_5O ($m/z = 45$) and identical signals with lower signal-to-noise ratio

TABLE 3: Summary of Reported Rate Constant Values for the Reaction $C_2H_5 + HO_2$

reaction	k/cm^3 mol^{-1} s^{-1}	method	ref
1, 1a	3.1×10^{13}	time-resolved MS	this work
1b	2.4×10^{13}	estimated	13
1d	3.0×10^{11}	estimated	13
1e	3.0×10^{11}	estimated	13
1a	3.0×10^{13}	modeling of a complex mechanism	20
1d	1.8×10^{12}	MS, very low-pressure reactor	21

were also obtained on the mass of $m/z = 45$. Because no interfering species are present in the $C_2H_6/H_2O_2/(COCl)_2$ reaction system, the mass signals at $m/z = 43$ and $m/z = 45$ should be fully attributable to the product C_2H_5O of reaction channel 1a. Moreover, the solid curve in Figure 6 represents a scaled numerical simulation of the C_2H_5O concentration−time profile based on the k_1 value and the reaction mechanism reported in this work. As expected for a direct product of reaction 1, the simulation and the experiment agree very well. However, because absolute concentrations of C_2H_5O have not yet been determined, a definite statement of the channel branching cannot be made at this stage.

4.3. Comparison with Previous Work. Table 3 summarizes the currently available kinetic information on reaction 1 and compares it with the result of our first direct determination of the total rate constant k_1. Tsang and Hampson[13] expected reaction 1b to be the most important product channel and estimated a rate constant of $k_{1b} = 2.4 \times 10^{13}$ cm^3 mol^{-1} s^{-1}, which agrees amazingly well with our direct measurement. They also estimated $k_{1d} = k_{1e} = 3.0 \times 10^{11}$ cm^3 mol^{-1} s^{-1}, showing that the H atom transfer channels are not important. Dobis and Benson,[21] on the other hand, measured the rate of reaction 1d by mass spectrometry in the reaction system $C_2H_6/O_2/Cl_2$ using a low-pressure reactor at millitorr pressures. The rate of reaction 1d was extracted from the observed concentrations of HO_2 and H_2O_2 in the reactor on the basis of a steady-state treatment of a rather complex reaction mechanism. Although the reported rate constant of $k_{1d} = 1.8 \times 10^{12}$ cm^3 mol^{-1} s^{-1} is much higher than the estimated value of Tsang and Hampson, this channel would still contribute merely a few percent to the total rate. Interestingly enough, the product of the assumed main channel (1a), C_2H_5O, could not be detected in their experiments. Finally, Bozelli and Dean[20] performed a QRRK study on the reaction $C_2H_5 + O_2$. Experimental literature data on that reaction could be successfully modeled by a complex mechanism assuming an additional fast HO_2 loss reaction according to reaction channel (1a). The reported rate constant, $k_{1a} = 3.0 \times 10^{13}$ cm^3 mol^{-1} s^{-1}, is in excellent agreement with our data; however, no further details on the modeling are given in their paper.

5. Conclusions

The overall rate constant of the radical−radical reaction $C_2H_5 + HO_2$ (1) has been measured for the first time. Controlled levels of HO_2 and C_2H_5 radicals were generated by 193 nm photolysis of mixtures of H_2O_2, C_2H_6, and $(COCl)_2$ in He. The thermal decomposition of an urea hydrogen peroxide adduct provided a reliable and stable H_2O_2 source. A perturbation approach was applied by measuring HO_2 and C_2H_5 concentration−time profiles by means of time-resolved mass spectrometry. Observed differences in the C_2H_5 signals measured without and with HO_2 present could be attributed mainly to the influence of the title reaction 1. The overall uncertainty of the rate determination was reduced by using HO_2 in large excess over C_2H_5 to provide for near pseudo-first-order conditions. An evaluation based on a comprehensive reaction mechanism (Table 1) resulted in a rate constant value of

$$k_1(293\ \mathrm{K}) = (3.1 \pm 1.0) \times 10^{13}\ \mathrm{cm^3\ mol^{-1}\ s^{-1}}$$

Strong mass signals of C_2H_5O were detected, indicating that channel (1a) with the products $C_2H_5O + OH$ is a major reaction channel. Measurements of the temperature dependence of the overall rate constant and extended product and branching fraction studies by means of laser induced fluorescence (LIF) are currently under way and will contribute to an improved understanding of the role of this reaction in low-temperature ignition processes.

Acknowledgment. This work was supported by the Deutsche Forschungsgemeinschaft and the Fonds der Chemischen Industrie. We acknowledge J. Gripp for help in setting up the new H_2O_2 source, and B. Brandt thanks T. Köcher for instructions for using the MS setup.

References and Notes

(1) Warnatz, J.; Maas, U.; Dibble, R. *Combustion*; Springer-Verlag: Berlin, Heidelberg, New York, 1996.

(2) Walker, R. W.; Morley, C. In *Basic Chemistry of Combustion,* in *Comprehensive Chemical Kinetics: Low-Temperature Combustion and Autoignition*; Pilling, M. J., Ed.; Elsevier: Amsterdam, 1997; Vol. 35.

(3) Ignatyev, S. I.; Xie, Y.; Allen, D. W.; Schaefer, H. F., III. *J. Chem. Phys.* **1997**, *107*, 141.

(4) Rienstra-Kiracofe, J. C.; Allen, W. D.; Schaefer, H. F., III. *J. Phys. Chem. A* **2000**, *104*, 9823.

(5) Carstensen, H. H.; N., C. V.; Anthony, M. D. *J. Phys. Chem. A* **2005**, *109*, 2264.

(6) Curran, H. J.; Gaffuri, P.; Pitz, W. J.; Westbrook, C. K. *Combust. Flame* **1998**, *114*, 149.

(7) Kazakov, A.; Zhao, Z.; Urban, B. D.; Dryer, F. L. *Int. Conf. Chemical Kinetics, 6th* **2005**, Abstract L15.

(8) Kee, R. J.; Ruply, F. M.; Miller, J. A. Chemkin-II: A Fortran Chemical Kinetics Package for the Analysis of Gas-Phase Chemical Kinetics; Sandia Report SAND89-8009; Sandia National Laboratories: Livermore, CA, 1989; http://www.ca.sandia.gov/chemkin/.

(9) Brandt, B. Untersuchungen von Radikalreaktionen im System Ethan, Methanol und Sauerstoff mit Hilfe der zeitaufgelösten Massenspektrometrie. Diploma thesis, Universität Kiel, 2004.

(10) Baklanov, A.; Krasnoperov, L. *J. Phys. Chem.* **2001**, *A 105*, 97.

(11) Atkinson, R.; Baulch, D. L.; Cox, R. A.; Crowley, N. J.; Hampson, J., R. F.; Hynes, R. G.; Jenkin, M. E.; Kerr, J. A.; Rossi, M. J.; Troe, J. *Summary of Evaluated Kinetic and Photochemical Data for Atmospheric Chemistry*; IUPAC Subcommittee on Gas Kinetic Data Evaluation for Atmospheric Chemistry; Web Version, July 2004.

(12) Baulch, D. L.; Cobos, C. J.; Cox, R. A.; Esser, C.; Frank, P.; Just, T.; Kerr, J. A.; Pilling, M. J.; Troe, J.; Walker, R. W.; Warnatz, J. *J. Phys. Chem. Ref. Data* **1992**, *21*, 411.

(13) Tsang, W.; Hampson, R. F. *J. Phys. Chem. Ref. Data* **1986**, *15*, 1087.

(14) Kaiser, E.; Rimai, L.; Wallington, T. *J. Phys. Chem.* **1989**, *93*, 4094.

(15) Fagerström, K.; Lund, A.; Mahmoud, G.; Jodowski, J.; Ratajczak, E. *Chem. Phys. Lett.* **1993**, *208*, 321.

(16) Atkinson, D. B.; Hudgens, J. W. *J. Phys. Chem. A* **1997**, *101*, 3901.

(17) Burcat, A.; Ruscic, B. Third Millenium Thermodynamic Database for Combustion and Air-Pollution Use with updates from Active Thermochemical Tables. Technol. rep.; Technion-IIT, Aerospace Engineering, and Argonne National Laboratory, Chemistry Division: Argonne, IL, 2005; http://ftp.technion.ac.il/pub/supported/aetdd/thermodynamics.

(18) Troe, J. *J. Chem. Soc., Faraday Trans.* **1994**, *90*, 2303.

(19) Caralp, F.; Devolder, P.; Fittschen, C.; Gomez, N.; Hippler, H.; Méreau, R.; Rayez, M. T.; Striebel, F.; Viskolcz, B. *Phys. Chem. Chem. Phys.* **1999**, *1*, 2935.

(20) Bozelli, J.; Dean, A. *J. Phys. Chem.* **1990**, *94*, 3313.

(21) Dobis, O.; Benson, S. *J. Am. Chem. Soc.* **1993**, *115*, 8798.